International Journal of Pharmaceutics 597 (2021) 120288

Contents lists available at ScienceDirect

International Journal of Pharmaceutics

journal homepage: www.elsevier.com/locate/ijpharm

Core-shell chitosan/PVA-based nanofibrous scaffolds loaded with *Satureja mutica* or *Oliveria decumbens* essential oils as enhanced antimicrobial wound dressing

Sajjad Barzegar [a], Mohammad Reza Zare [a], Fatemeh Shojaei [a], Zahra Zareshahrabadi [b], Omid Koohi-Hosseinabadi [c], Mohammad Jamal Saharkhiz [d], Aida Iraji [e], Kamiar Zomorodian [b,f,*], Mohammad Khorram [a,*]

[a] Department of Chemical Engineering, School of Chemical and Petroleum Engineering, Shiraz University, Shiraz, Iran
[b] Department of Medical Mycology and Parasitology, School of Medicine, Shiraz University of Medical Sciences, Shiraz, Iran
[c] Central Research Laboratory, Shiraz University of Medical Sciences, Shiraz, Iran
[d] Department of Horticultural Sciences, Collage of Agriculture, Shiraz University, Shiraz, Iran
[e] Medicinal and Natural Products Chemistry Research Center, Shiraz University of Medical Sciences, Shiraz, Iran
[f] Basic Sciences in Infectious Diseases Research Center, Shiraz University of Medical Sciences, Shiraz, Iran

ARTICLE INFO

Keywords:
Wound healing
Antibacterial activity
Coaxial electrospinning
Satureja mutica
Oliveria decumbens
Antioxidant activity

ABSTRACT

Wounds are prone to bacterial infections, which cause a delayed healing process. Regarding the emergence of bacterial resistance to common antibiotics, using natural antimicrobial agents can be beneficial. Chitosan is a biological polymer, which has shown partial antioxidant and antimicrobial activities. In this study, core-shell nanofibrous scaffolds composed of chitosan (CS)/polyvinyl alcohol (PVA) as the core and polyvinylpyrrolidone (PVP)/ maltodextrin (MD) as the shell were developed. *Satureja mutica* (*S. mutica*) or *Oliveria decumbens* (*O. decumbens*) essential oil (EO) was encapsulated into the core of the produced scaffolds. The broth microdilution analysis showed significant antimicrobial activity of the EOs. The SEM analysis indicated that the unloaded and loaded core-shell scaffolds with *S. mutica* or *O. decumbens* EO had a uniform, beadless structure with fiber mean diameters of 210 ± 50, 250 ± 45, and 225 ± 46 nm, respectively. The CS/PVA-PVP/MD and CS/PVA/EO-PVP/MD scaffolds indicated suitable mechanical properties. The addition of the studied EOs enhanced the antioxidant activity of the scaffolds. The antimicrobial test of produced scaffolds showed that loading of 10% *S. mutica* or *O. decumbens* EO could broaden the microbicidal activity of the CS/PVA-PVP/MD scaffolds. These results revealed that the CS/PVA/EO-PVP/MD nanofibrous scaffolds are promising candidates for wound dressing.

1. Introduction

Skin regulates body temperature, protects it from microorganism invasion, and provides sensory functions (Memic et al., 2019; Shi et al., 2018). However, the skin is prone to severe damages due to diabetic ulcers, burn injuries, chronic wounds, etc. (López Angulo and do Amaral Sobral, 2016; Movahedi et al., 2020). When wounds occur, it is susceptible to the invasion of microorganisms (Yang et al., 2017), and the subsequent infection of the wound complicates the healing process (Kandhasamy et al., 2017). Wounds pass through the inflammatory phase, proliferation phase, and collagen and granule formation stages to heal (Dubský et al., 2012). However, the bacterial infection hinders these phases; thus, a steady and constant dose of antibacterial agents is demanded to overcome this challenge (Dhand et al., 2017).

The production of cytokines and the promotion of immune cells occur during the inflammatory phase. Cytokines provoke fibroblast and chondrocyte cells to manufacture reactive oxygen species (ROS) (Volpe et al., 2018). However, the uncontrolled level of ROSs causes cell damage. Since a sustained low-level presence of the ROSs is required for wound healing, the regulation of the amount of the ROSs with an

* Corresponding authors at: Department of Medical Mycology and Parasitology, School of Medicine, Shiraz University of Medical Sciences, Shiraz, Iran (K. Zomorodian). School of Chemical and Petroleum Engineering, Shiraz University, Shiraz, Iran (M. Khorram).
E-mail addresses: zomorodian@sums.ac.ir (K. Zomorodian), mkhorram@shirazu.ac.ir (M. Khorram).

https://doi.org/10.1016/j.ijpharm.2021.120288
Received 27 September 2020; Received in revised form 16 January 2021; Accepted 17 January 2021
Available online 26 January 2021
0378-5173/

appropriate antioxidant compound is essential to healing the wound (El-Aassar et al., 2020).

To overcome the mentioned challenges, the local treatment of wounds is more practical. Because its independence from the circulation system allows a high concentration of bioactive agents with low systemic toxicity (Chen et al., 2017; Ojah et al., 2019). Recently, wound dressings such as hydrogels, cellulose sponges, and nanofibrous scaffolds have been proposed to protect wounds from the invasion of microorganisms, provide a humid environment, transmit oxygen, and release bioactive agents (Bakhsheshi-Rad et al., 2020; Nguyen et al., 2013; Ojah et al., 2019; Zhang et al., 2019a). Nanofibrous scaffolds have gained a lot of interest in recent years. Such scaffolds possess a high specific surface area, a large number of interconnected pores, flexibility, and lightweight (El-Aassar et al., 2016; Karuppuswamy et al., 2014; Zhang et al., 2019a). These aspects allow the scaffolds to emulate the functions of the extracellular matrix, which are mechanical support and cell activity regulation (Fang et al., 2019; Rho et al., 2006). In addition, bioactive compounds such as antibacterial and antioxidant agents can be readily loaded into the scaffolds and exhibit an appropriate release of the compounds (Li et al., 2018; Pavliňáková et al., 2018). Nanofibrous scaffolds have been manufactured through template synthesis, self-assembly, drawing, and phase separation techniques. However, the lack of controllability over these methods and improper nanofiber formation have restricted their application (Jithendra et al., 2013; Karuppuswamy et al., 2014). Electrospinning is a convenient method that allows the production of long and continuous fibers with tunable diameters (Sofi et al., 2019). This technique enables modifying porosity, pore size, and fiber diameter of nanofibrous scaffolds. The pre-process parameters such as type of polymers and solvents, and their concentration in the solution affect these parameters. Moreover, the process parameters like voltage intensity and collector distance from the needle can be altered to control the features of nanofibrous scaffolds (Choi et al., 2008; Santoro et al., 2016). Earlier, the electrospinning was capable of forming uniaxial nanofibrous scaffolds. The uniaxial structure of scaffolds often exhibits a burst release profile of the loaded bioactive agent. Coaxial electrospinning technique has solved this challenge. The core–shell structure resultant from this technique enables the encapsulation of the curative agent into the core layer, and then the shell layer controls its release profile. Besides, the core–shell nanofibers show better mechanical strength (Movahedi et al., 2020; Ojah et al., 2019; Santoro et al., 2016).

Both synthetic and natural polymers are required to produce nanofibrous scaffolds using electrospinning. Synthetic polymers provide mechanical strength, and natural polymers assist cellular adhesion and growth (Kim et al., 2009). Chitosan (CS) is a naturally derived polysaccharide that promotes cell adhesion and cellular growth (Naeimi et al., 2020). Moreover, this polymer possesses antibacterial and antioxidant effects (Ahmed et al., 2018). It has been reported that a combination of polyvinyl alcohol (PVA) with CS in wound dressing could enhance the mechanical strength and provides a humid environment for wounds (Naeimi et al., 2020). Polyvinylpyrrolidone (PVP) is another polymer that introduces the hydrophilic character. This polymer allows a suitable release rate of hydrophobic drugs and increases the drug concentration at the treatment site (Li et al., 2018). In addition to the polymers, bioactive compounds are usually loaded to the scaffolds to meet the antibacterial and antioxidant requirements (Ghorbani et al., 2020). The bacterial drug resistance to some antibiotics and toxicity of some of their alternatives like silver nanoparticles have caused the human return to the herbal extracts (Shi et al., 2018; Sofi et al., 2019). Phytochemicals are valuable sources of novel drug development. These compounds possess antibacterial, hemostasis, anti-inflammatory, and re-epithelization effects that can promote the healing process (Kandhasamy et al., 2017; Sofi et al., 2019). Previous studies have reported that *Satureja mutica* (*S. mutica*) and *Oliveria decumbens* (*O. decumbens*) essential oils (EOs) contain considerable amounts of thymol and carvacrol (Esmaeili et al., 2018; Ghorbanpour et al., 2016). These two oxygenated monoterpenes possess great antimicrobial and antioxidant activities (Fonseca et al., 2019; Marchese et al., 2016).

Since the electrospinning of CS is difficult and owns low mechanical strength (Yan et al., 2014), this research aimed to use a CS/PVA mixture as a core layer and enhance its mechanical properties by covering it with a shell layer containing PVP and MD. Furthermore, the *S. mutica* or *O. decumbens* EO was added to the core layer of the nanofibers in the quest for promoting its antimicrobial and antioxidant properties. To achieve these goals and prevent the burst release of the EOs, the coaxial electrospinning method was used to encapsulate the active agents. The physicochemical, antibacterial, and antioxidant analysis of CS/PVA-PVP/MD core–shell nanofibrous scaffolds containing each of the two EOs were carried out to investigate the efficacy of produced nanofibrous scaffold.

2. Materials and methods

2.1. Materials

PVP (Mw 360000) was purchased from Fluka. PVA (Mw 72000) and acetic acid (purity $\geq$ 99%) were obtained from Merck Co, Germany. CS (50–190 kDa, 75–85% deacetylated) was provided from Sigma-Aldrich (USA), and MD (DE $<$ 20) was purchased from Zar Fructose Co, Iran. *S. mutica* seeds and *O. decumbens* plants were obtained from the school of agriculture, Shiraz University. Sabouraud dextrose agar (SDA) and Brain heart infusion (BHI) were purchased from Merck. Co, Germany.

2.2. Preparation of essential oils

The *S. mutica* seeds and *O. decumbens* plants were air-dried and then powdered in a mixer, separately. The powdered seeds and plants were hydro-distilled for 4 h using the Clevenger type apparatus. The collected essential oils were dried over anhydrous sodium sulfate and stored in sealed vials at 4 °C until use.

2.3. Gas chromatography–mass spectrometry (GC–MS) analysis

Gas chromatography-mass spectrometry was carried out to analyze the chemical composition of the *S. mutica* and *O. decumbens* EOs using Agilent-7890A coupled to Agilent 7000 mass spectrometer equipped with a DB-1MS capillary column (30.00 m $\times$ 0.25 mm, 0.25 μm film thickness). Helium was selected as a carrier gas at a flow rate of 1.2 ml/min. The GC conditions were programmed to increase the temperature from 70 to 280 °C at the rate of 3 °C/min and finally held at 280 °C for 4 min. The samples (0.1 μl) were injected with a split ratio of 1:30 with a temperature of 250 °C. The transfer line temperature was 280 °C. The quadrupole mass spectrometer was taken in electron impact (EI) mode (70 eV) in the m/z range of 40–600. The relative percentage values were calculated from the total area under the peaks by the software of the apparatus. Compounds were identified by studying their spectral data and retention indices with Wiley Mass Spectral Data 7th edition, NIST Mass Spectral Library, and Adams, 2007.

2.4. Antimicrobial activity of S. Mutica and O. Decumbens EOs

2.4.1. Microorganisms

In the current study, standard strains of bacteria and fungi, including *Pseudomonas aeruginosa* (ATCC 9027), *Escherichia coli* (ATCC 25922), *Staphylococcus aureus* (ATCC 25923), *Candida dubliniensis* (CBS 8501), and *Candida albicans* (ATCC 10261) were used.

2.4.2. Minimum inhibitory concentration

The minimum inhibitory concentration (MIC) values of *S. mutica* and *O. decumbens* EOs were determined using the broth microdilution method suggested by clinical and laboratory standards institute. Briefly, a serial dilution of the both EOs with concentrations ranging from

0.0625 μl/ml to 32 μl/ml was prepared in 96-well microliter plates using the Müller-Hinton broth and RPMI-1640 (Sigma, USA) for bacteria and fungi, respectively. Cell densities were adjusted to 0.5 McFarland standards at 630 nm wavelength (stock suspension of 1–1.5 × 10^8 CFU/ml for bacteria and 1–5 × 10^6 CFU/ml for fungi). Following that, 100 μl of the microbial suspension was added in each well of columns 2–12. The first column (200 μl of the uninoculated medium) was included as a sterility control. The plates were incubated at 37 °C (bacteria) and 32 °C (fungi) for 24–48 h. After incubation, the MIC values were visually observed and defined as the lowest concentration of the EOs that produced no visible growth. All experiments were performed in duplicate.

To determine the minimum microbicidal concentration (MMC) values of bacterial and fungal strains, 10 μl of media from all wells showing no visible growth was cultured on BHI (bacteria) and SDA (fungi) plates. After incubation overnight, the MMC values were determined as the lowest concentration that showed either no growth or less than four colonies.

2.5. Preparation of electrospinning solution

To prepare electrospinning solutions, 6% w/v of PVA was dissolved into deionized (DI) water at 80 °C followed by stirring for 3 h. The CS solution was prepared by dissolving 2% w/v of CS in acetic acid. After completely dissolving, the CS solution was added to the PVA solution in a final concentration of 30% v/v of acetic acid and stirred for overnight. The prepared solution was used as the core solution. For shell solution, MD and PVP were dissolved into DI water at the concentrations of 5% w/v and 10% w/v, respectively. In addition, to prepare EO loaded nanofibrous scaffolds, *S. mutica* or *O. decumbens* EO at the concentration of 10% were added to the core solution and mixed for an additional 24 h. After mixing, the color of solution turned from transparent to white, which shows the formation of emulsion. The PVA in the emulsified solution act as stabilizer (Coker, 1957; Feng and Huang, 2013; Kemala et al., 2012), and the emulsion was stable after 72 h. It is worth noting that previous studies have shown the stability and antimicrobial activity of EOs in acidic conditions did not considerably change (Kim et al., 2004; Lv et al., 2017; Nguefack et al., 2004; Si et al., 2009).

2.6. Coaxial electrospinning

In order to produce core–shell nanofibers, coaxial electrospinning was carried out using a dual pump electrospinning machine. First, the prepared polymer solutions were loaded into two 10 ml syringes equipped with a coaxial spinning needle. To attain the smooth and beads free nanofibers, the solutions were electrospun at different combinations of 0.5 and 0.6 ml/h shell flow rates and 0.1 and 0.2 ml/h core flow rates. The DC power source applied a high voltage of 21 kV. The rotary drum collector was wrapped with a 20 × 20 cm aluminum foil, and the distance of the collector was kept 15 cm away from the needle tip. After selecting the proper conditions, the prepared core solution containing each of the EOs and the shell solution were electrospun. The produced nanofibrous mats stored in sealed coverings at 4 °C for further analysis.

2.7. Characterization of electrospun scaffolds

2.7.1. Scanning electron microscopy (SEM) & transmission electron microscopy (TEM)

The morphology of core–shell nanofibrous scaffolds was determined using a SEM (TESCAN-Vega 3, Czech Republic). The samples of scaffolds (1 cm^2) were sputter-coated with gold for 120 s before observation in order to decrease the charging effect. The images with different magnifications were captured to create a better view of fibers' morphology. In addition, the scaffolds loaded with EOs were also observed to evaluate the effect of EOs on the morphology and diameter size of nanofibers. The ImageJ software (National Institute of Health, USA) was used to measure the diameter size of the nanofibers. The average diameters of prepared nanofibers were determined by measuring diameters of 50 fibers, which were selected randomly.

TEM (TEM Leo 912 omega, Zeiss, Germany) was used to confirm the formation of core–shell nanofibers. The nanofiber samples were prepared by placing a lacey carbon-coated copper grid on the collector prior to the examination.

2.7.2. Fourier transform infrared (FTIR) spectroscopy analysis

The samples were analyzed by a FTIR spectroscopy (Bruker, Germany) with a scan range of 500–3500 cm^{-1} at 4 cm^{-1} resolution to evaluate their chemical composition.

2.7.3. Mechanical strength

The mechanical properties of the optimum nanofibrous scaffolds and their combinations with EOs were evaluated using a universal testing machine (SANTAM, STM20, Iran) with a load capacity of 500 N. To perform this examination based on the ASTM standard test method D882-02 (ASTM, 2002), rectangular samples of the scaffolds with a dimension of 50 mm × 10 mm were prepared and stretched at a crosshead speed of 5 mm/min. The assay was carried out triplicate.

2.7.4. Loading capacity and encapsulation efficiency

The loading capacity (LC) and encapsulation efficiency (EE) of the nanofibrous mats were determined by measuring the amount of entrapped EOs in the nanofibrous mats according to Zhang et al. with some modifications (Zhang et al., 2019b). Briefly, the CS/PVA/EO-PVP/MD mats were dissolved in a 50% (v/v) ethanol aqueous solution. After complete dissolving, the amount of entrapped EOs were measured using a UV–Vis spectrophotometer (Cary 100 UV–vis, Agilent, USA). The assay was performed triplicate. The wavelengths of 276 nm (*O. decumbens* EO) and 279 nm (*S. mutica* EO) were utilized for plotting the standard calibration curves. The CS/PVA-PVP/MD nanofibrous mat (without EO) was selected as a blank for this assay. The LC and EE were calculated by using following equations:

$$LC(\%) = \frac{The\ \ amount\ \ of\ \ entrapped\ \ EO\ \ in\ \ mat\ \ (g)}{Weight\ \ of\ \ mat\ \ (g)} \times 100 \quad (1)$$

$$EE(\%) = \frac{The\ \ amount\ \ of\ \ entrapped\ \ EO\ \ in\ \ mat\ \ (g)}{Theoritical\ \ EO\ \ (g)} \times 100 \quad (2)$$

Where *Theoretical EO* is the amount of EO in the core solution.

2.8. Antioxidant activity

The antioxidant activity of the nanofiber samples was evaluated using the Diphenyl-2-picrylhydrazyl (DPPH) radical scavenging assay. A 200 mg sample of each of the produced nanofibrous scaffolds was immersed in 1 ml methanol and vortexed for about 15 min. The prepared samples were further diluted with MeOH at different concentrations. 20 μl of the solutions and 180 μl of a methanolic solution of DPPH (110 μM) were mixed in a 96-well plate and incubated in the dark for 30 min. Then, their absorbance was measured spectrophotometrically at 517 nm. All the tests were repeated three times. The results were reported as average± standard deviation and compared to the quercetin as a standard.

The antioxidant activity was calculated as follows:

$$Antioxidant\ \ activity(\%) = \frac{Abs\ \ control - Abs\ \ sample}{Abs\ \ control} \times 100 \quad (3)$$

Where *Abs control* and *Abs sample* represent the absorbance of DPPH radical with methanol and the absorbance of DPPH radical with nanofibers, respectively.

2.9. Antimicrobial activity of scaffolds

The antimicrobial activities of the produced electrospun scaffolds

were assessed against standard strains of *Pseudomonas aeruginosa* (ATCC 9027), *Escherichia coli* (ATCC 25922), *Staphylococcus aureus* (ATCC 25923), *Candida dubliniensis* (CBS 8501), and *Candida albicans* (ATCC 10261), according to the standard AATCC 100 test method (Ardekani et al., 2019). In brief, the produced unloaded scaffold and scaffolds containing EOs were cut into circular swatches (2.5 cm in diameter) and sterilized under UV light for 30 min. After that, 1000 μl of microorganism suspension at cell densities of 0.5 McFarland was added into falcon tubes containing scaffolds. Then, the sterilized scaffolds were incubated with the microorganism suspensions for 24 h. After that contact time, 10 ml phosphate-buffered saline (PBS, pH = 7.4) was added to the falcon tubes and shaken for about 60 s. Subsequently, 10 μl of the solution was cultured on an appropriate medium and placed at 37 °C for 24 h. This procedure was carried out in triplicate. The viable colonies were counted, and then the reduction percent of microorganism was calculated by the following equation:

$$Reduction(\%) = \frac{A - B}{A} \times 100 \quad (4)$$

Where A is the number of microorganisms that grew on the agar plates for untreated control, and B is the number of microorganisms recovered from inoculated nanofibrous scaffolds after 24 h.

2.10. Statistical analysis

The investigated data are reported as mean ± SD. The student's *t*-test method was used to analyze the reported data. Statistical differences were considered significant when p-value < 0.05.

3. Results and discussion

3.1. GC–MS spectroscopy

The GC–MS analysis of *S. mutica* and *O. decumbens* EOs were performed to establish their chemical composition. According to Table 1, the *S. mutica* EO contained 44 compounds. The major component of this EO was carvacrol (64.036%). Following that, ρ-cymene (12.105%), γ-terpinene (6.22%), thymol (2.244), and α-terpinene (2.027%) showed considerable concentrations. Other studies have revealed almost similar results. Sefidkon and Jamzad reported that the major components of *S. mutica* EO were carvacrol (30.9%), thymol (26.5%), γ-terpinene (14.9%), and ρ-cymene (10.3%) (Sefidkon and Jamzad, 2005). Another research showed that the *S. mutica* EO derived from Tangegol (Golestan, Iran) contained mostly carvacrol (70.4%), borneol (10.5%), thymol (6.5%), and ρ-cymene (3.5%) (Karimi et al., 2016). The obtained results revealed that the concentration of oxygenated monoterpenes, particularly carvacrol, in the *S. mutica* EO was noticeable.

As Table 1 depicts, the chemical composition of *O. decumbens* EO comprised 21 ingredients. The most abundant components were γ-terpinene (25.87%), thymol (20.32%), carvacrol (18.77%), ρ-cymene (12.72%), myristicin (9.89%), and limonene (5.5%). A previous study on *O. decumbens* EO showed that thymol (28.45%), γ-terpinene (22.2%), ρ-cymene (17.90%), myristicin (13.55%), carvacrol (8.50%), and limonene (2.60%) were dominant (Alizadeh Behbahani et al., 2018). Another investigation on the *O. decumbens* EO composition at various phenological stages showed that ρ-cymene, γ-terpinene, thymol, and carvacrol were major components (Esmaeili et al., 2018). Therefore, the results of this study were comparable with the others, and the slight difference in the composition of EOs could be related to the numerous reasons such as the plants' phenology stage, climatic conditions, collection process, and geographical origin (Alizadeh Behbahani et al., 2018).

3.2. Antimicrobial activity of S. Mutica and O. Decumbens EOs

The GC–MS analysis of *S. mutica* and *O. decumbens* EOs revealed mainly the presence of oxygenated monoterpenes such as carvacrol and thymol. These ingredients of essential oils possess potential antibacterial activity (Vitanza et al., 2019). Therefore, the investigation on the microbicidal activity of *S. mutica* and *O. decumbens* EOs against standard strains of *P. aeruginosa*, *E. coli*, *S. aureus*, *C. dubliniensis*, and *C. albicans* were evaluated by CLSI protocol. As Table 2 reveals, the MIC values ranged from 0.0625 to 4 μl/ml for *S. mutica* EO and 0.125 to 8 μl/ml for *O. decumbens* EO, and the MMC values varied from 0.0625 to 16 μl/ml and 1 to 32 μl/ml, respectively.

These results demonstrated that these two EOs have an excellent ability to inhibit the growth of bacteria and fungi species. The antibacterial results of the *S. mutica* EO were close to that of other researches. For instance, the study performed on this EO revealed its minimum bactericidal concentrations against *E. coli*, *S. aureus*, and

Table 1
The chemical composition of *Satureja mutica* and *Oliveria decumbens* essential oil.

	Components	RI[1]	Area (%)	Components	RI	Area (%)	Components	RI	Area (%)
***S. mutica* EO**	(E)-2-Hexenal	850	0.12	(Z)-b-Ocimene	1036	0.097	**Carvacrol**	**1299**	**64.036**
	Tricyclene	923	0.024	(E)-b-Ocimene	1046	0.158	Unknown	1324	0.212
	α-Thujene	926	0.07	**γ-Terpinene**	**1059**	**6.22**	Carvacrol acetate	1374	0.06
	α-Pinene	933	0.38	Unknown	1079	0.047	α-Copaene	1376	0.079
	Camphene	948	0.257	Terpinolene	1089	0.925	(Z)-Caryophyllene	1408	0.109
	Thuja-2,4(10)-diene	953	0.021	Linalool	1099	0.265	(E)-Caryophyllene	1419	0.276
	1-Octen-3-ol	977	1.189	n-Nonanal	1105	0.01	γ-Muurolene	1476	0.137
	Myrcene	991	0.853	1-Octen-3-yl acetate	1112	0.011	Viridiflorene	1494	0.145
	3-Octanol	995	0.078	Borneol	1165	0.618	α-Muurolene	1500	0.212
	ρ-Phellandrene	1004	0.341	Terpinen-4-ol	1177	0.304	β-Bisabolene	1509	0.48
	ρ-Mentha-1(7),8-diene	1007	0.063	a-Terpineol	1190	0.069	γ-Cadinene	1514	0.22
	α-Terpinene	**1017**	**2.027**	Methyl chavicol	1198	1.801	δ-Cadinene	1523	0.481
	ρ-Cymene	**1026**	**12.105**	Carvacrol methyl ether	1244	0.088	α-Cadinene	1537	0.052
	Limonene	1029	0.783	Thymoquinone	1254	1.005	Thymohydro quinone	1557	0.729
	1,8-Cineole	1031	0.598	**Thymol**	**1291**	**2.244**			
	Components	**RI**	**Area (%)**	**Components**	**RI**	**Area (%)**	**Components**	**RI**	**Area (%)**
***O. decumbens* EO**	α-Thujene	930	0.28	**ρ-Cymene**	**1024**	**12.72**	α-Terpineol	1188	0.04
	α-Pinene	939	0.15	**Limonene**	**1029**	**5.5**	Carvacrol methyl ether	1244	0.31
	Camphene	954	0.19	β-Phellandrene	1030	0.41	**Thymol**	**1290**	**20.32**
	Sabinene	975	1.9	(E)-β-Ocimene	1050	0.07	**Carvacrol**	**1299**	**18.77**
	β-Myrcene	991	0.46	**γ-Terpinene**	**1059**	**25.87**	Thymol acetate	1352	0.09
	α-Phellandrene	1002	0.02	Terpinolene	1088	0.05	**Myristicin**	**1518**	**9.89**
	γ-3-Carene	1011	0.04	Terpinen-4-ol	1177	0.15	Elemicin	1557	2.75

[1] RI: Retention Index.

Table 2
Antimicrobial activities of *Satureja mutica* and *Oliveria Decumbens* essential oil by broth microdilution method.

	Organisms	ATCC/ CBS	*Satureja Mutica* EO		*Oliveria decumbens* EO	
			MIC[1] (µl / ml)	MMC[2] (µl / ml)	MIC (µl / ml)	MMC (µl / ml)
Bacterial Strains	*Staphylococcus aureus*	ATCC 25923	4	4	4	8
	Escherichia coli	ATCC 25922	2	2	4	4
	Pseudomonas aeruginosa	ATCC 9027	4	16	8	32
Fungal Strains	*Candida albicans*	ATCC 10261	1	2	2	4
	Candida dubliniensis	CBS 8501	0.0625	0.0625	0.125	1

[1] MIC: minimum inhibitory concentration;
[2] MMC: minimum microbicidal concentration.

P. aeruginosa strains were 8, 2, and 8 µl/ml, respectively (Ghorbanpour et al., 2016). Another study showed that the MMC values of *S. mutica* EO against respective microorganisms were 2, 8, and > 64 µl/ml (Hadian et al., 2012). In comparison, this survey resulted that *S. mutica* EO could kill *E. coli*, *S. aureus*, and *P. aeruginosa* bacteria at concentrations of 2, 4, and 16 µl/ml, respectively. The slight difference between these results may be related to the dissimilarity in their composition. In this research, *S. mutica* EO contained a remarkable concentration of carvacrol (64.036%), based on GC–MS results. The pure carvacrol has antimicrobial effects against various microorganisms, especially *S. aureus* and *E. coli.* This activity is related to the high hydrophobicity of carvacrol that leads to the debilitating of the cell membrane (Ben Arfa et al., 2006). Thus, the lower MIC values of *S. mutica* compared to other studies might be related to its higher content of carvacrol. Also, the antibacterial activities of *O. decumbens* EO against *E.coli* and *P. aeruginosa* were almost similar to a previous study. (Alizadeh Behbahani et al., 2018).

According to Table 2, both the EOs exhibited potent activity against Gram-positive and Gram-negative bacteria, although previous researches have shown that EOs have a greater inhibitory effect against Gram-positive bacteria than Gram-negative strains (Victoria et al., 2012; Zomorodian et al., 2017). The high bactericidal effect of EOs against Gram-positive bacteria could be due to the permeability of hydrophobic molecules through their cell walls. As a result, the phenolic compounds of essential oils could adversely affect the cell wall and cytoplasmic contents. Due to the outer membrane of the Gram-negative bacteria, which results in its relative impermeability, they are more resistant to EOs. However, the thymol and carvacrol contents of EOs can indirectly disintegrate the bacterial outer membrane of Gram-negative strains and bring about its death (Nazzaro et al., 2013).

Altogether, the significant bactericidal activity of *S. mutica* and *O. decumbens* EOs could be attributed to the high phenolic contents (Table 1). Furthermore, the higher sensitivity of microorganisms against the *S. mutica* EO compared to the *O. decumbens* EO could be related to its higher concentration of carvacrol. In addition, *S. mutica* and *O. decumbens* EOs showed a strong potential to inhibit the growth of *Candida* strains. These antifungal activities could broaden the antimicrobial effect of these EOs and inhibit further infections. As a result, these two essential oils could be used to inhibit the growth of probable infecting microorganisms, particularly the *S. aureus* strains that are the most common cause of wound infection in the world (Dhand et al., 2017).

3.3. Characterization of core–shell nanofibrous scaffolds

3.3.1. Morphology

Previous studies revealed that the electrospinning of the CS, when used alone, is difficult because of its low solubility, strong hydrogen bonds, and polycationic features. To solve this problem, researchers combined CS with other polymers to become electrospinnable. On the other hand, single nozzle electrospinning results in burst release of loaded drugs in drug delivery applications (Yan et al., 2014). In this research to overcome these problems, the core–shell nanofibrous scaffolds composed of CS/PVA/EO as the core and PVP/MD as the shell was fabricated by the coaxial electrospinning method. First, different core and shell flow rates were examined to obtain beadless and homogeneous nanofibers (Table 3). The SEM images of these scaffolds were evaluated at different magnifications and are shown in Fig. 1**.** This figure illustrates that all the nanofibers are unaligned. Previous studies showed that the unaligned structure of nanofibers promotes O_2 permeation and cellular proliferation (Lee et al., 2017). Also, the SEM images exhibited little conglutination of the fibers, which may be related to the fast vaporization of the solvents. According to Table 3, the diameter of primary samples (S1, S2, S3, and S4) did not show a considerable difference and were 183 ± 43, 216 ± 50, 210 ± 50, and 222 ± 49 nm, respectively. The relatively thin diameter of the core–shell scaffolds is correlated to the ionic polyelectrolyte feature of their ingredients. Due to this trait, the polymer solution had a higher charge density on the tip of the ejected jet of the electrospinning; therefore, induced higher elongation force and finally decreased the fiber diameter (Sajeev et al., 2008). The smaller nanofiber diameter brings about the larger ratio of surface area to volume (Yousefi et al., 2017). The higher surface area per mass of nanofibrous scaffolds is significant because it can provide better release of the loaded drug (Shokrollahi et al., 2020). Although the S1 nanofiber sample had the thinnest fiber diameter, it contained beads that restricted its functionality. As a result, because the S3 nanofiber sample had beadless and smaller fiber diameters compared to other primary ones, the preparation conditions of this sample were chosen for further investigations and incorporation with bioactive agents.

According to Table 3, the addition of *S. mutica* or *O. decumbens* EO slightly increased the fiber diameter. This result was the same as the obtained results by Torabi Ardekani et al. on CS/PVA based nanofibrous scaffolds loaded with *Zataria multiflora* EO (Ardekani et al., 2019). The S3-10% *S. mutica* and S3-10% *O. decumbens* scaffolds had a fiber mean diameter of 250 ± 45 and 225 ± 46 nm, respectively. This insignificant rise in the fiber size of EO loaded scaffolds might be the result of a change in the viscosity of feed solution due to the addition of EOs. The diameters of nanofibers were between the range of 50 to 500 nm, which is the size of collagen fibers of ECM (Choi et al., 2008). Moreover, Fig. 2 demonstrates that the morphology of nanofibrous scaffolds incorporated with *S. mutica* or *O. decumbens* EO was similar to the S3 sample structure. Therefore, the diameter size, alignment, and smoothness of these scaffolds make them suitable for wound dressing applications.

The TEM analysis was carried out to evaluate the core–shell structure of nanoscale fibers. Fig. 3 shows that the core–shell structure formed successfully. The interface between these two layers determines that the shell appropriately encapsulates the core section. The high contrast difference between the two layers resulted from the unequal density of the core (CS/PVA) and the shell (PVP/MD) solutions. Thus, the coaxial electrospinning apparatus properly produced the nanoscale core–shell fibers.

Table 3
The mean diameter of nanofibrous scaffolds at different core–shell flow rates.

Sample	Flow rate (ml/h)		Mean diameter (nm)
	Core	Shell	
S1	0.2	0.5	183 ± 43
S2	0.1	0.5	216 ± 50
S3	0.2	0.6	210 ± 50
S4	0.1	0.6	222 ± 49
S3-10% *S. mutica*	0.2	0.6	250 ± 45
S3-10% *O. decumbens*	0.2	0.6	225 ± 46

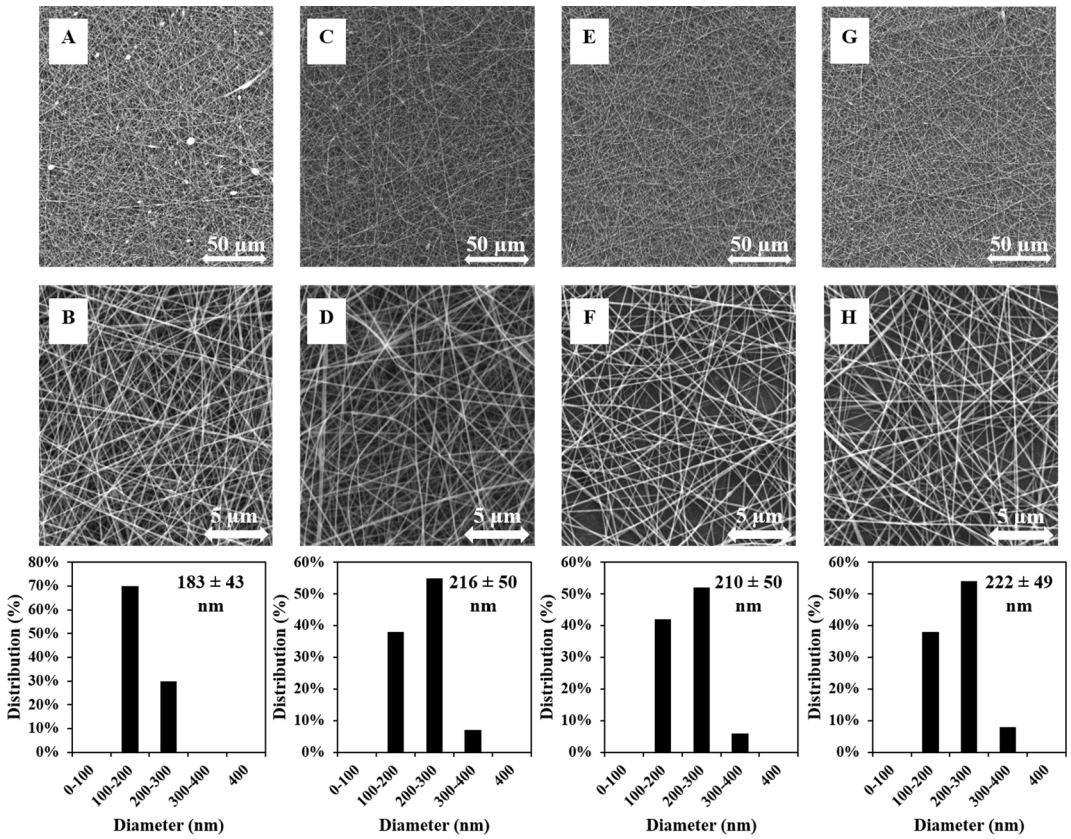

Fig. 1. The SEM images of primary nanofibrous scaffolds at different core and shell flow rates (A, B) S1 sample, (C, D) S2 sample, (E, F) S3 sample, and (G, H) S4 sample. Magnification: A, C, E, and G = 1 kx, B, D, F, and H = 10 kx.

3.3.2. FTIR analysis

The FTIR analysis was performed to investigate the probable interactions among components of the produced scaffolds. The FTIR spectra of the CS, PVA, PVP, MD, and the prepared nanofibrous scaffolds are shown in Fig. 4. CS exhibited a peak at 3355 cm^{-1} revealing the presence of N-H, O-H, and its relative intermolecular hydrogen forces. The characteristic peak at 1589 cm^{-1} was attributed to the amide groups of CS. In addition, the C-H and C-O bonds were evident from the peaks at 1374 and 1150 cm^{-1}, respectively (Hadipour-Goudarzi et al., 2014). The FTIR analysis of MD showed the peaks at 3283, 2888, and 1602 cm^{-1}, which corresponded to the O-H, C-H, and C-O stretching vibrations, respectively. Also, the peaks ranged from 520 to 992 cm^{-1} showed the skeletal vibrations of the pyranoid ring (Kang et al., 2019). The FTIR spectrum of PVA resulted in the O-H, C-H, H-C-OH, and C-O bonds peaked at the 3330, 2947, 1422, and 1092 cm^{-1}, correspondingly (Alavarse et al., 2017). The PVP powder was characterized by the C-H, C=O, and C-N bonds at the respective peaks of 2948, 1652, and 1283 cm^{-1} (Tawfik et al., 2020).

The spectra of the S3 scaffold showed that all the utilized polymers existed in the S3 sample. As evident in Fig. 4, the O-H peak of the S3 sample slightly differed from the other materials and a little broadened. This change may have resulted from hydrogen bonding occurring between N-H and O-H groups that existed in CS, PVA, and MD. This result was in agreement with previous studies (Hadipour-Goudarzi et al., 2014; Li et al., 2018). The addition of 10% *O. decumbens* or *S. mutica* EO to the core layer of the S3 scaffolds did not produce new peaks. As Fig. 4 indicates, the intensity of O-H and C-H stretching increased due to the presence of alcoholic components of the EOs. The similar results were concluded by other researchers (Fonseca et al., 2019; Keawchaoon and Yoksan, 2011; Lin et al., 2018). This effect was more significant on the FTIR spectrum of the S3-10% *S. mutica* than that of the S3-10% *O. decumbens* because *S. mutica* EO contained higher amounts of phenolic compounds (like thymol and carvacrol). Therefore, the FTIR analysis proved the appropriate fabrication of the intended scaffolds.

3.3.3 Mechanical strength

The produced nanofibrous scaffold must have sufficient mechanical strength to be acceptable in tissue engineering applications. The mechanical properties of the scaffolds containing 10% *S. mutica* or *O. decumbens* EO were investigated to ensure its performance. In Table 4, the ultimate tensile strength (UTS), elongation at break (EB), and Young's modulus (YM) of the tested scaffolds are presented.

The S3 scaffold showed UTS of 8.92 ± 0.1 MPa and YM of 487.81 ± 48.9 MPa. These values were higher than the scaffolds composed of CS/PVA or even cross-linked ones, which were evaluated in previous studies (Liao et al., 2011). The higher UTS and YM of the S3 sample compared with un-cross-linked and cross-linked nanofibrous scaffolds suggested that the shell layer containing PVP/MD could appropriately heighten the mechanical strength of scaffolds. Previous studies also showed that the core–shell structure had the potential to heighten the mechanical properties of nanofibrous scaffolds (Afshar et al., 2019; Chen et al., 2010). Also, the higher mechanical strength could be related to the hydrogen bonding of the shell materials with core polymers, as seen in the FTIR analysis.

Based on Table 4, the UTS and YM of scaffolds loaded with EOs declined while their EB increased. These changes are because of the plasticizing effect of herbal extracts and their impact on the hydrogen-bonding network of nanofiber materials, which was in accordance with FTIR results (Adeli-Sardou et al., 2019; Almasian et al., 2020). In addition, Afshar et al. expressed that the rise in the nanofiber diameter could weaken its tensile strength (Afshar et al., 2019). Since the SEM results showed the scaffolds loaded with EOs had higher mean diameter, this might have decreased their UTS and YM properties. Moreover, the comparison between the mechanical properties of the S3-10% *S. mutica*

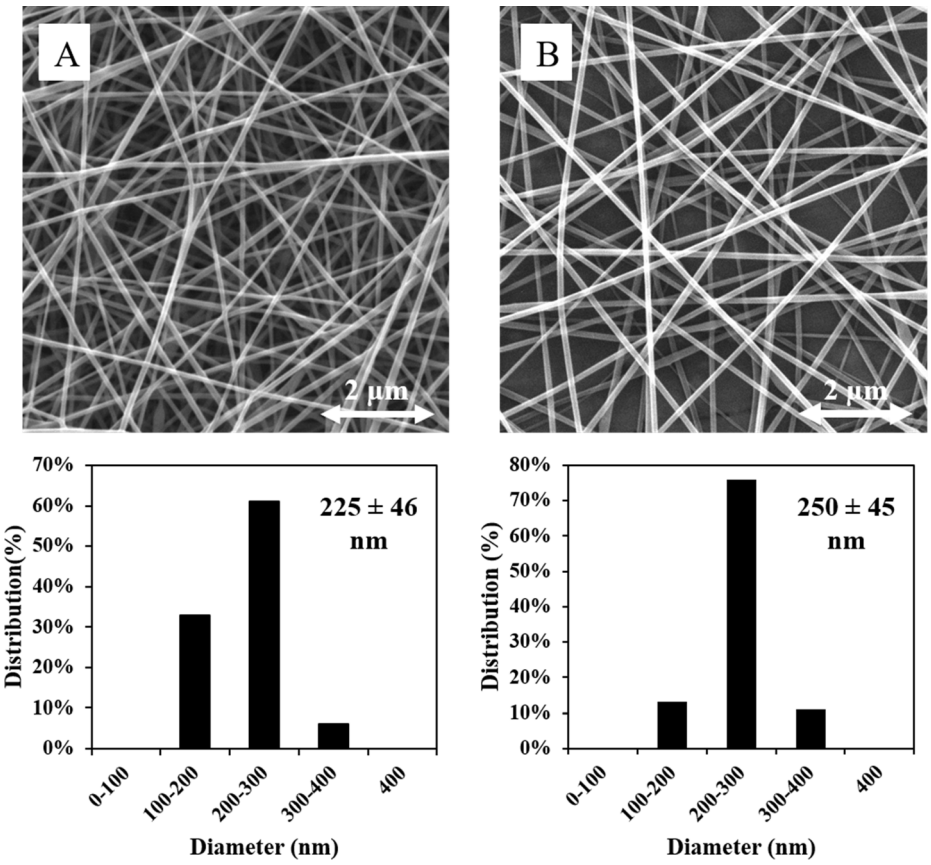

Fig. 2. The SEM images of (A) S3-10% *O. decumbens* and (B) S3-10% *S. mutica* at 20 kx magnification.

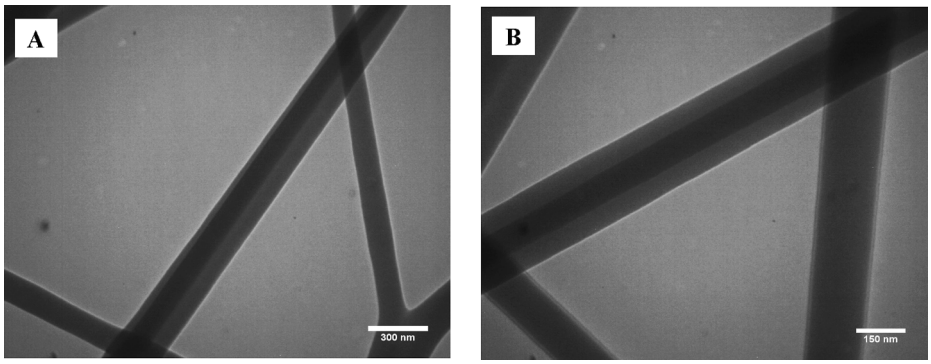

Fig. 3. The TEM images of S3 scaffold (A) 300 nm scale and (B) 150 nm scale.

and the S3-10% *O. decumbens* nanofibrous scaffolds demonstrated that the addition of *S. mutica* EO more strongly impacted the amounts of UTS, YM, and EB than *O. decumbens* EO. This difference might be correlated to higher carvacrol concentration of *S. mutica* EO; as Fonseca et al. concluded that increasing in carvacrol concentration could decline the elastic behavior of nanofibers (Fonseca et al., 2019). However, the tensile strength of all the examined scaffolds was between 0.8 and 18 MPa, the range that was suggested for nanofibrous scaffolds to be compatible for wound dressing applications (Yousefi et al., 2017).

3.3.4. Loading capacity and encapsulation efficiency

Evaluating the amount of LC and EE are essential to confirm and quantify the encapsulation of essential oils (Osanloo et al., 2020). The obtained results showed that the LC of S3-10% *S. mutica* and S3-10% *O. decumbens* were 9.14 ± 0.42% and 8.99 ± 0.28%, respectively. Also, the EE amounts of *S. mutica* or *O. decumbens* EO-loaded mats were 82.90 ± 6.37% and 80.10 ± 4.04%, respectively. According to Tampau et al (2020), the relatively high EE can be correlated with the high viscosity of solution that restricts emulsion destabilization during evaporation of the solvent. Besides, the interactions between EOs and PVA in the core solution help the EOs to be entrapped in the nanofibers (Tampau et al., 2020).

3.4. Antioxidant activity of scaffolds

The antioxidant activity could play a key role in wound healing by minimizing reactive oxygen species (ROS) (Sarhan et al., 2016; Thangavel et al., 2018). In the current study, the antioxidant capacity of the scaffolds was investigated using the DPPH assay, and the results are given in Table 5. The antioxidant activity of the loaded scaffolds with the EOs was significantly improved compared to the blank scaffold (S3 sample). As indicated in Table 5, 80 mg/ml of the S3-10% *S. mutica* and

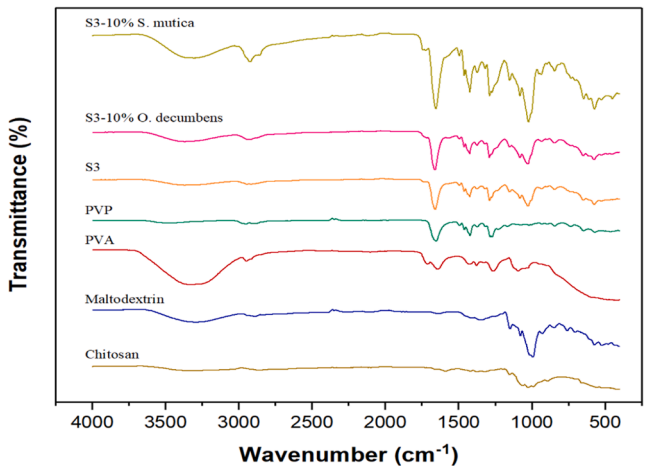

Fig. 4. The FTIR results of Chitosan, Maltodextrin, PVA, and PVP powders and S3, S3-10% *O. decumbens* and S3-10% *S. mutica* nanofibrous scaffolds.

Table 4
The mechanical properties of the S3 sample and the S3 contained 10% *S. mutica* or *O. decumbens* essential oil. (mean ± SD, p-value < 0.05, n = 3).

Sample	Ultimate Tensile strength (MPa)	Elongation at break (%)	Yong's modulus (MPa)
S3[a]	8.92 ± 0.1	2.73 ± 0.05	487.81 ± 48.9
S3-10% *S. mutica*[b]	4.68 ± 0.07	3.7 ± 0.06	243.6 ± 20.2
S3-10% *O. decumbens*[c]	7.73 ± 0.08	3.51 ± 0.08	405.45 ± 34.4
Statistic (p-value < 0.05)	a,b and a,c	a,b and a,c	–

Table 5
Antioxidant activities of the electrospun scaffolds measured by the DPPH. The values are given as mean ± SD (p-value < 0.05, n = 3).

Sample	Inhibition percentage ± SD			IC_{50} (mg/ml) ± SD
	80 mg/ml	40 mg/ml	20 mg/ml	
S3	18.07 ± 0.95	11.35 ± 1.10	9.41 ± 2.06	–
S3-10% *O. decumbens*	61.74 ± 3.20*	47.31 ± 1.54	28.19 ± 4.41	46.17 ± 2.20
S3-10% *S. mutica*	64.12 ± 5.55*	48.42 ± 0.44*	31.02 ± 3.59	43.50 ± 3.33
Quercetin	–	–	–	16.98 ± 0.54 μM

* p-value < 0.05

the S3-10% *O. decumbens* scavenged 64.12 ± 5.55% and 61.74 ± 3.20% of the free radicals (p-value < 0.05, n = 3), respectively. Also, the inhibition values were enhanced in a dose-dependent manner. This high antioxidant activity of the scaffolds loaded with EOs was due to the presence of alcoholic monoterpene and phenolic compounds, which possess hydrogen and electron donor ability (Aytac et al., 2016). In addition, the S3-10% *S. mutica* indicated higher amounts of inhibition compared to the S3-10% *O. decumbens*, which might be due to the higher value of oxygenated monoterpenes (carvacrol and thymol) in the *S. mutica* (Abou Baker et al., 2020). Furthermore, the S3-10% *S. mutica* and the S3-10% *O. decumbens* showed the IC_{50} values of 43.50 ± 3.33 and 46.17 ± 2.25 mg/ml, respectively.

Consequently, the high antioxidant property of the S3-10% *S. mutica* and the S3-10% *O. decumbens* could make them promising candidates for wound dressing.

3.5. Antimicrobial properties of scaffolds

The bactericidal activity of the produced scaffolds was measured using colony count and compared with control (Fig. 5). The antimicrobial results of the nanofibrous scaffolds with and without essential oils are presented in Fig. 6. The S3 scaffold partially reduced the growth of bacteria strains, while it did not affect *Candida* strains (Fig. 6). These results were almost the same as the others conducted from the study performed by Torabi Ardekani et al. (Ardekani et al., 2019). The bactericidal activity of the CS/PVA-PVP/MD scaffold might be related to its CS content. Previously, other studies showed that the polycationic trait of CS, which is due to the presence of NH2 groups, induces the electrostatic attraction between the scaffold and negatively charged bacterial cell membranes. This action weakens the wall integrity of the cell and causes its death (Masood et al., 2019; Singh et al., 2018). Also, it has been reported that the combination of CS and PVA could enhance the bactericidal activity of nanofibrous scaffolds (Jacob et al., 2019). Fig. 6 illustrates that the antibacterial activity of the S3 scaffold against Gram-negative bacteria strains (*E. coli* and *P. aeruginosa*) was greater than Gram-positive (*S. aureus*). This effect could be related to the electrostatic force between the CS polymer and the cell wall of Gram-negative bacteria. The amine group of CS strongly bonds to the surface of Gram-negative bacteria and causes cell leakage. However, the interaction between Gram-positive bacteria and CS could generate a barrier and restricts nutrient supply to the cell (Yousefi et al., 2017). Previous researches on the anti-*Candida* effect of different types of chitosan revealed that the minimum inhibitory concentration of CS should be at least 1 mg/ml to be effective (Tayel et al., 2010). Since the concentration of CS in the culture solutions was lower than that, the little anti-*Candida* effect of the S3 scaffold was predictable.

As can be seen in Fig. 6, the addition of *S. mutica* or *O. decumbens* EO significantly heightened the antimicrobial activity of the produced scaffolds and completely inhibited the growth of microorganism strains. As mentioned earlier, the microbicidal activity of the EOs is related to their phenolic compounds. These ingredients affect cell membrane integrity and cause cell lysis (Nazzaro et al., 2013). Furthermore, it has been reported that carvacrol (the major component of *S. mutica* EO) could disturb the ion and pH equilibria of the cell cytoplasm and induce a microbicide effect (Fonseca et al., 2019). According to the results of the LC analysis, the concentrations of EOs in the incubated solutions of microorganisms with swatches were about 3.9 μl/ml. The higher microbicidal effect of EOs loaded in nanofibers in comparison to that of the pure EOs against the tested microorganisms could be related to the chitosan antibacterial activity. Besides, the combination of chitosan with EOs might have resulted in a synergistic effect. These results are accordance with the previous studies that have shown synergistic antimicrobial activity of chitosan with EOs (Wang et al., 2011; Yuan et al., 2016).

The antimicrobial results showed that the produced scaffolds containing *O. decumbens* or *S. mutica* EO inhibited the growth of both the Gram-positive and Gram-negative bacteria along with *Candida* species. This broad range of antimicrobial effect could protect the wound site from a probable wound infection.

4. Conclusion

In the current research, CS/PVA-PVP/MD nanofibrous scaffolds loaded with *S. mutica* or *O. decumbens* EO were appropriately electrospun to produce the core–shell structure. The mechanical analysis showed that the properties of the fabricated scaffolds enhanced compared to the previously produced CS/PVA-based scaffolds by other researchers. Furthermore, the results of the GC–MS test revealed that oxygenated monoterpenes were the main components of *S. mutica* and *O. decumbens* EOs. This result may explain the considerable MIC and MMC values of these EOs, which further resulted in the enhancement of the antimicrobial activity of CS/PVA-based scaffolds against

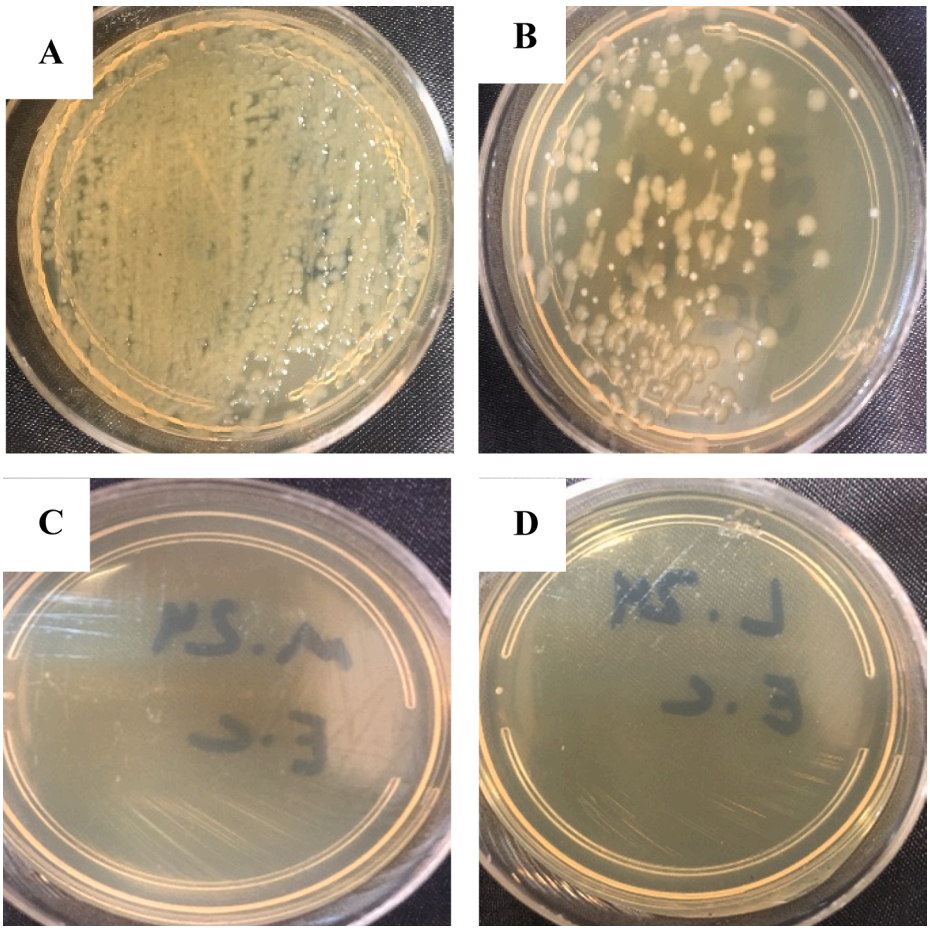

Fig. 5. The antibacterial activity of produced scaffolds against *E. coli* bacteria (A) Control, (B) S3, (C) S3-10% *O. decumbens*, (D) S3-10% *S. mutica*.

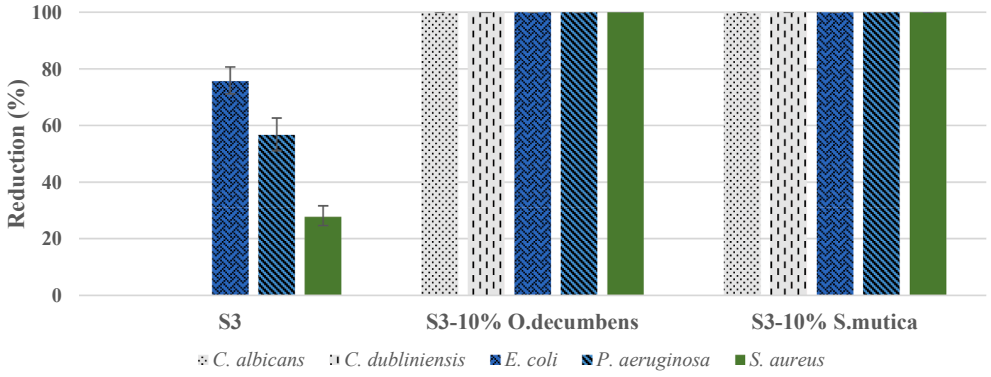

Fig. 6. The antimicrobial activity of S3 sample and the S3 contained 10% *S. mutica* and *O. decumbens* essential oils against mentioned microorganisms after 24 h contact time. The data are exhibited as mean ± SD (p-value < 0.05, $n = 3$).

P. aeruginosa, *E. coli*, *S. aureus*, *C. dubliniensis*, and *C. albicans*. Also, the addition of the *S. mutica* or *O. decumbens* EO to the core–shell nanofibrous scaffolds increased the antioxidant activity of nanofibers from 18.07 ± 0.95 to 64.12 ± 5.55 and 61.74 ± 3.20 percentage at 80 mg/ml concentration, respectively. In conclusion, the *S. mutica* and *O. decumbens* EO modified the antimicrobial and antioxidant activities of the CS/PVA-based scaffolds. The core–shell nanofibrous scaffolds loaded with each of the EOs can be potentially utilized as dressings for dry wounds because of their suitable mechanical properties, antioxidant effect, and antimicrobial activities. According to the obtained results, in future research, nanofibers with stability in aqueous media can be produced by selecting a suitable cross-linking agent and then, its properties for the treatment of moist wounds can be investigated.

CRediT authorship contribution statement

Sajjad Barzegar: Data curation, Investigation, Writing - original draft. **Mohammad Reza Zare:** Data curation, Investigation, Methodology. **Fatemeh Shojaei:** Investigation. **Zahra Zareshahrabadi:** Writing - review & editing. **Omid Koohi-Hosseinabadi:** Investigation. **Mohammad Jamal Saharkhiz:** Investigation. **Aida Iraji:** Methodology. **Kamiar Zomorodian:** Conceptualization, Project administration, Supervision. **Mohammad Khorram:** Conceptualization, Project administration, Supervision.

Declaration of Competing Interest

The authors declare that they have no known competing financial interests or personal relationships that could have appeared to influence the work reported in this paper.

Acknowledgment

This study was partially funded by Shiraz University of Medical Sciences. The authors would like to thank Ms. Hasti Nouraei for her invaluable assistance in the antimicrobial analysis.

References

Abou Baker, D.H., Al-Moghazy, M., ElSayed, A.A.A., 2020. The in vitro cytotoxicity, antioxidant and antibacterial potential of Satureja hortensis L. essential oil cultivated in Egypt. Bioorg. Chem. 95, 103559. https://doi.org/10.1016/j.bioorg.2019.103559.

Adeli-Sardou, M., Yaghoobi, M.M., Torkzadeh-Mahani, M., Dodel, M., 2019. Controlled release of lawsone from polycaprolactone/gelatin electrospun nano fibers for skin tissue regeneration. Int. J. Biol. Macromol. Elsevier B.V. 124, 478–491. https://doi.org/10.1016/j.ijbiomac.2018.11.237.

Afshar, S., Rashedi, S., Nazockdast, H., Ghazalian, M., 2019. Preparation and characterization of electrospun poly(lactic acid)-chitosan core-shell nanofibers with a new solvent system. Int. J. Biol. Macromol. 138, 1130–1137. https://doi.org/10.1016/j.ijbiomac.2019.07.053.

Ahmed, R., Tariq, M., Ali, I., Asghar, R., Noorunnisa Khanam, P., Augustine, R., Hasan, A., 2018. Novel electrospun chitosan/polyvinyl alcohol/zinc oxide nanofibrous mats with antibacterial and antioxidant properties for diabetic wound healing. Int. J. Biol. Macromol. 120, 385–393. https://doi.org/10.1016/j.ijbiomac.2018.08.057.

Alavarse, A.C., de Oliveira Silva, F.W., Colque, J.T., da Silva, V.M., Prieto, T., Venancio, E.C., Bonvent, J.J., 2017. Tetracycline hydrochloride-loaded electrospun nanofibers mats based on PVA and chitosan for wound dressing. Mater. Sci. Eng. C 77, 271–281. https://doi.org/10.1016/j.msec.2017.03.199.

Alizadeh Behbahani, B., Tabatabaei Yazdi, F., Vasiee, A., Mortazavi, S.A., 2018. Oliveria decumbens essential oil: Chemical compositions and antimicrobial activity against the growth of some clinical and standard strains causing infection. Microb. Pathog. 114, 449–452. https://doi.org/10.1016/j.micpath.2017.12.033.

Almasian, A., Najafi, F., Eftekhari, M., Ardekani, M.R.S., Sharifzadeh, M., Khanavi, M., 2020. Polyurethane/carboxymethylcellulose nanofibers containing Malva sylvestris extract for healing diabetic wounds: Preparation, characterization, in vitro and in vivo studies. Mater. Sci. Eng. C 114, 111039. https://doi.org/10.1016/j.msec.2020.111039.

Ardekani, N.T., Khorram, M., Zomorodian, K., Yazdanpanah, S., Veisi, H.H., Veisi, H.H., 2019. Evaluation of electrospun poly (vinyl alcohol)-based nanofiber mats incorporated with Zataria multiflora essential oil as potential wound dressing. Int. J. Biol. Macromol. 125, 743–750. https://doi.org/10.1016/j.ijbiomac.2018.12.085.

Aytac, Z., Kusku, S.I., Durgun, E., Uyar, T., 2016. Encapsulation of gallic acid/cyclodextrin inclusion complex in electrospun polylactic acid nanofibers: Release behavior and antioxidant activity of gallic acid. Mater. Sci. Eng. C 63, 231–239. https://doi.org/10.1016/j.msec.2016.02.063.

Bakhsheshi-Rad, H.R., Ismail, A.F., Aziz, M., Akbari, M., Hadisi, Z., Omidi, M., Chen, X., 2020. Development of the PVA/CS nanofibers containing silk protein sericin as a wound dressing: In vitro and in vivo assessment. Int. J. Biol. Macromol. 149, 513–521. https://doi.org/10.1016/j.ijbiomac.2020.01.139.

Ben Arfa, A., Combes, S., Preziosi-Belloy, L., Gontard, N., Chalier, P., 2006. Antimicrobial activity of carvacrol related to its chemical structure. Lett. Appl. Microbiol. 43 (2), 149–154. https://doi.org/10.1111/lam.2006.43.issue-210.1111/j.1472-765X.2006.01938.x.

Chen, R., Huang, C., Ke, Q., He, C., Wang, H., Mo, X., 2010. Preparation and characterization of coaxial electrospun thermoplastic polyurethane/collagen compound nanofibers for tissue engineering applications. Colloids Surf. B Biointerfaces 79 (2), 315–325. https://doi.org/10.1016/j.colsurfb.2010.03.043.

Chen, S., Liu, B., Carlson, M.A., Gombart, A.F., Reilly, D.A., Xie, J., 2017. Recent advances in electrospun nanofibers for wound healing. Nanomedicine 12 (11), 1335–1352. https://doi.org/10.2217/nnm-2017-0017.

Choi, J.S., Leong, K.W., Yoo, H.S., 2008. In vivo wound healing of diabetic ulcers using electrospun nanofibers immobilized with human epidermal growth factor (EGF). Biomaterials 29 (5), 587–596. https://doi.org/10.1016/j.biomaterials.2007.10.012.

Coker, J.N., 1957. Poly(vinyl Alcohol) as an Emulsifying Agent in Vinyl Polymerizations. Ind. Eng. Chem. 49 (3), 382–385. https://doi.org/10.1021/ie51392a030.

Dhand, C., Venkatesh, M., Barathi, V.A., Harini, S., Bairagi, S., Goh Tze Leng, E., Muruganandham, N., Low, K.Z.W., Fazil, M.H.U.T., Loh, X.J., Srinivasan, D.K., Liu, S.P., Beuerman, R.W., Verma, N.K., Ramakrishna, S., Lakshminarayanan, R., 2017. Bio-inspired crosslinking and matrix-drug interactions for advanced wound dressings with long-term antimicrobial activity. Biomaterials 138, 153–168. https://doi.org/10.1016/j.biomaterials.2017.05.043.

Dubský, M., Kubinová, Š., Širc, J., Voska, L., Zajíček, R., Zajícová, A., Lesný, P., Jirkovská, A., Michálek, J., Munzarová, M., Holáň, V., Syková, E., 2012. Nanofibers prepared by needleless electrospinning technology as scaffolds for wound healing. J. Mater. Sci. Mater. Med. 23 (4), 931–941. https://doi.org/10.1007/s10856-012-4577-7.

El-Aassar, M.R., El fawal, G.F., El-Deeb, N.M., Hassan, H.S., Mo, X., 2016. Electrospun Polyvinyl Alcohol/ Pluronic F127 Blended Nanofibers Containing Titanium Dioxide for Antibacterial Wound Dressing. Appl. Biochem. Biotechnol. 178 (8), 1488–1502. https://doi.org/10.1007/s12010-015-1962-y.

El-Aassar, M.R., Ibrahim, O.M., Fouda, M.M.G., El-Beheri, N.G., Agwa, M.M., 2020. Wound healing of nanofiber comprising Polygalacturonic/Hyaluronic acid embedded silver nanoparticles: In-vitro and in-vivo studies. Carbohydr. Polym. 238, 116175. https://doi.org/10.1016/j.carbpol.2020.116175.

Esmaeili, H., Karami, A., Maggi, F., 2018. Essential oil composition, total phenolic and flavonoids contents, and antioxidant activity of Oliveria decumbens Vent. (Apiaceae) at different phenological stages. J. Clean. Prod. 198, 91–95. https://doi.org/10.1016/j.jclepro.2018.07.029.

Fang, Y., Zhu, X., Wang, N., Zhang, X., Yang, D., Nie, J., Ma, G., 2019. Biodegradable core-shell electrospun nanofibers based on PLA and γ-PGA for wound healing. Eur. Polym. J. 116, 30–37. https://doi.org/10.1016/j.eurpolymj.2019.03.050.

Feng, S.S., Huang, G., 2013. Effects of emulsifiers on the controlled release of paclitaxel (taxol ®) from nanospheres of biodegradable polymers. Chemother. Eng. Collect. Pap. Si-Shen Feng - A Tribut. to Shu Chien His 82nd Birthd. 71, 307–336. https://doi.org/10.4032/9789814463157.

Fonseca, L.M., Cruxen, C.E.D.S., Bruni, G.P., Fiorentini, Â.M., Zavareze, E.d.R., Lim, L.-T., Dias, A.R.G., 2019. Development of antimicrobial and antioxidant electrospun soluble potato starch nanofibers loaded with carvacrol. Int. J. Biol. Macromol. 139, 1182–1190. https://doi.org/10.1016/j.ijbiomac.2019.08.096.

Ghorbani, M., Nezhad-Mokhtari, P., Ramazani, S., 2020. Aloe vera-loaded nanofibrous scaffold based on Zein/Polycaprolactone/Collagen for wound healing. Int. J. Biol. Macromol. 153, 921–930. https://doi.org/10.1016/j.ijbiomac.2020.03.036.

Ghorbanpour, M., Hadian, J., Hatami, M., Salehi-Arjomand, H., Aliahmadi, A., 2016. Comparison of chemical compounds and antioxidant and antibacterial properties of various Satureja species growing wild in Iran. J. Med. Plants 15, 58–72.

Hadian, J., Akramian, M., Heydari, H., Mumivand, H., Asghari, B., 2012. Composition and invitro antibacterial activity of essential oils from four Satureja species growing in Iran. Nat. Prod. Res. 26, 98–108. https://doi.org/10.1080/14786419.2010.534734.

Hadipour-Goudarzi, E., Montazer, M., Latifi, M., Aghaji, A.A.G., 2014. Electrospinning of chitosan/sericin/PVA nanofibers incorporated with in situ synthesis of nano silver. Carbohydrate Polym. Elsevier Ltd. 113, 231–239. https://doi.org/10.1016/j.carbpol.2014.06.082.

Jacob, J., Peter, G., Thomas, S., Haponiuk, J.T., Gopi, S., 2019. Chitosan and polyvinyl alcohol nanocomposites with cellulose nanofibers from ginger rhizomes and its antimicrobial activities. Int. J. Biol. Macromol. 129, 370–376. https://doi.org/10.1016/j.ijbiomac.2019.02.052.

Jithendra, P., Rajam, A.M., Kalaivani, T., Mandal, A.B., Rose, C., 2013. Preparation and characterization of aloe vera blended Collagen-Chitosan composite scaffold for tissue engineering applications. ACS Appl. Mater. Interfaces 5 (15), 7291–7298. https://doi.org/10.1021/am401637c.

Kandhasamy, S., Perumal, S., Madhan, B., Umamaheswari, N., Banday, J.A., Perumal, P. T., Santhanakrishnan, V.P., 2017. Synthesis and Fabrication of Collagen-Coated Ostholamide Electrospun Nanofiber Scaffold for Wound Healing. ACS Appl. Mater. Interfaces 9 (10), 8556–8568. https://doi.org/10.1021/acsami.6b1648810.1021/acsami.6b16488.s001.

Kang, Y.R., Lee, Y.K., Kim, Y.J., Chang, Y.H., 2019. Characterization and storage stability of chlorophylls microencapsulated in different combination of gum Arabic and maltodextrin. Food Chem. 272, 337–346. https://doi.org/10.1016/j.foodchem.2018.08.063.

Karimi, E., Ghasemnezhad, A., Hadian, J., Ghorbanpour, M., 2016. Assessment of essential oil constituents and main agro-morphological variability in Satureja mutica populations. Rev. Bras. Bot. 39 (1), 77–85. https://doi.org/10.1007/s40415-015-0215-1.

Karuppuswamy, P., Venugopal, J.R., Navaneethan, B., Laiva, A.L., Sridhar, S., Ramakrishna, S., 2014. Functionalized hybrid nanofibers to mimic native ECM for tissue engineering applications. Appl. Surf. Sci. 322, 162–168. https://doi.org/10.1016/j.apsusc.2014.10.074.

Keawchaoon, L., Yoksan, R., 2011. Preparation, characterization and in vitro release study of carvacrol-loaded chitosan nanoparticles. Colloids Surf. B Biointerfaces 84 (1), 163–171. https://doi.org/10.1016/j.colsurfb.2010.12.031.

Kemala, T., Budianto, E., Soegiyono, B., 2012. Preparation and characterization of microspheres based on blend of poly(lactic acid) and poly(ε-caprolactone) with poly (vinyl alcohol) as emulsifier. Arab. J. Chem. 5, 103–108. https://doi.org/10.1016/j.arabjc.2010.08.003.

Kim, J.A.Y.W., Kim, Y.S., Kyung, K.Y.U.H., 2004. Inhibitory Activity of Essential Oils of Garlic and Onion against Bacteria and Yeasts 67, 499–504.

Kim, S.E., Heo, D.N., Lee, J.B., Kim, J.R., Park, S.H., Jeon, S.H., Kwon, I.K., 2009. Electrospun gelatin/polyurethane blended nanofibers for wound healing. Biomed. Mater. 4 (4), 044106. https://doi.org/10.1088/1748-6041/4/4/044106.

Lee, N.M., Erisken, C., Iskratsch, T., Sheetz, M., Levine, W.N., Lu, H.H., 2017. Polymer fiber-based models of connective tissue repair and healing. Biomaterials 112, 303–312. https://doi.org/10.1016/j.biomaterials.2016.10.013.

Li, J.J., Yang, Y.Y., Yu, D.G., Du, Q., Yang, X.L., 2018. Fast dissolving drug delivery membrane based on the ultra-thin shell of electrospun core-shell nanofibers. Eur. J. Pharm. Sci. 122, 195–204. https://doi.org/10.1016/j.ejps.2018.07.002.

Liao, H., Qi, R., Shen, M., Cao, X., Guo, R., Zhang, Y., Shi, X., 2011. Improved cellular response on multiwalled carbon nanotube-incorporated electrospun polyvinyl alcohol/chitosan nanofibrous scaffolds. Colloids Surf. B Biointerfaces 84 (2), 528–535. https://doi.org/10.1016/j.colsurfb.2011.02.010.

Lin, L., Zhu, Y., Cui, H., 2018. Electrospun thyme essential oil/gelatin nanofibers for active packaging against Campylobacter jejuni in chicken. Lwt 97, 711–718. https://doi.org/10.1016/j.lwt.2018.08.015.

López Angulo, D.E., do Amaral Sobral, P.J., 2016. Characterization of gelatin/chitosan scaffold blended with aloe vera and snail mucus for biomedical purpose. Int. J. Biol. Macromol. 92, 645–653. https://doi.org/10.1016/j.ijbiomac.2016.07.029.

Lv, Xia, Liu, Tiantian, Ma, Huipeng, Tian, Yan, Li, Lei, Li, Zhen, Gao, Meng, Zhang, Jianbin, Tang, Zeyao, 2017. Preparation of Essential Oil-Based Microemulsions for Improving the Solubility, pH Stability. Photostabil., Skin Permeation of Quercetin 18 (8), 3097–3104. https://doi.org/10.1208/s12249-017-0798-x.

Marchese, A., Orhan, I.E., Daglia, M., Barbieri, R., Di Lorenzo, A., Nabavi, S.F., Gortzi, O., Izadi, M., Nabavi, S.M., 2016. Antibacterial and antifungal activities of thymol: A brief review of the literature. Food Chem. 210, 402–414. https://doi.org/10.1016/j.foodchem.2016.04.111.

Masood, N., Ahmed, R., Tariq, M., Ahmed, Z., Masoud, M.S., Ali, I., Asghar, R., Andleeb, A., Hasan, A., 2019. Silver nanoparticle impregnated chitosan-PEG hydrogel enhances wound healing in diabetes induced rabbits. Int. J. Pharm. 559, 23–36. https://doi.org/10.1016/j.ijpharm.2019.01.019.

Memic, Adnan, Abudula, Tuerdimaimaiti, Mohammed, Halimatu S., Joshi Navare, Kasturi, Colombani, Thibault, Bencherif, Sidi A., 2019. Latest Progress in Electrospun Nanofibers for Wound Healing Applications. ACS Appl. Bio Mater. 2 (3), 952–969. https://doi.org/10.1021/acsabm.8b00637.

Movahedi, M., Asefnejad, A., Rafienia, M., Khorasani, M.T., 2020. Potential of novel electrospun core-shell structured polyurethane/starch (hyaluronic acid) nanofibers for skin tissue engineering: In vitro and in vivo evaluation. Int. J. Biol. Macromol. 146, 627–637. https://doi.org/10.1016/j.ijbiomac.2019.11.233.

Naeimi, Atena, Payandeh, Maryam, Ghara, Abdollah Ramzani, Ghadi, Fereshteh Ezzati, 2020. In vivo evaluation of the wound healing properties of bio-nanofiber chitosan/polyvinyl alcohol incorporating honey and Nepeta dschuparensis. Carbohydr. Polym. 240, 116315. https://doi.org/10.1016/j.carbpol.2020.116315.

Nazzaro, F., Fratianni, F., De Martino, L., Coppola, R., De Feo, V., 2013. Effect of essential oils on pathogenic bacteria. Pharmaceuticals 6, 1451–1474. https://doi.org/10.3390/ph6121451.

Nguefack, J., Leth, V., Zollo, P.H.A., Mathur, S.B., 2004. Evaluation of five essential oils from aromatic plants of Cameroon for controlling food spoilage and mycotoxin producing fungi 94, 329–334. https://doi.org/10.1016/j.ijfoodmicro.2004.02.017.

Nguyen, Thuy Thi Thu, Ghosh, Chiranjit, Hwang, Seong-Gu, Tran, Lam Dai, Park, Jun Seo, 2013. Characteristics of curcumin-loaded poly (lactic acid) nanofibers for wound healing. J. Mater. Sci. 48 (20), 7125–7133. https://doi.org/10.1007/s10853-013-7527-y.

Ojah, N., Saikia, D., Gogoi, D., Baishya, P., Ahmed, G.A., Ramteke, A., Choudhury, A.J., 2019. Surface modification of core-shell silk/PVA nanofibers by oxygen dielectric barrier discharge plasma: Studies of physico-chemical properties and drug release behavior. Appl. Surf. Sci. 475, 219–229. https://doi.org/10.1016/j.apsusc.2018.12.270.

Osanloo, Mahmoud, Arish, Javad, Sereshti, Hassan, 2020. Developed methods for the preparation of electrospun nanofibers containing plant-derived oil or essential oil: a systematic review. Polym. Bull. 77 (11), 6085–6104. https://doi.org/10.1007/s00289-019-03042-0.

Pavliňáková, V., Fohlerová, Z., Pavliňák, D., Khunová, V., Vojtová, L., 2018. Effect of halloysite nanotube structure on physical, chemical, structural and biological properties of elastic polycaprolactone/gelatin nanofibers for wound healing applications. Mater. Sci. Eng. C 91, 94–102. https://doi.org/10.1016/j.msec.2018.05.033.

Rho, Kyong Su, Jeong, Lim, Lee, Gene, Seo, Byoung-Moo, Park, Yoon Jeong, Hong, Seong-Doo, Roh, Sangho, Cho, Jae Jin, Park, Won Ho, Min, Byung-Moo, 2006. Electrospinning of collagen nanofibers: Effects on the behavior of normal human keratinocytes and early-stage wound healing. Biomaterials 27 (8), 1452–1461. https://doi.org/10.1016/j.biomaterials.2005.08.004.

Sajeev, U.S., Anoop Anand, K., Menon, Deepthy, Nair, Shanti, 2008. Control of nanostructures in PVA, PVA/chitosan blends and PCL through electrospinning. Bull. Mater. Sci. 31 (3), 343–351. https://doi.org/10.1007/s12034-008-0054-9.

Santoro, M., Shah, S.R., Walker, J.L., Mikos, A.G., 2016. Poly(lactic acid) nanofibrous scaffolds for tissue engineering. Adv. Drug Deliv. Rev. 107, 206–212. https://doi.org/10.1016/j.addr.2016.04.019.

Sarhan, Wessam A., Azzazy, Hassan M.E., El-Sherbiny, Ibrahim M., 2016. Honey/Chitosan Nanofiber Wound Dressing Enriched with Allium sativum and Cleome droserifolia: Enhanced Antimicrobial and Wound Healing Activity. ACS Appl. Mater. Interfaces 8 (10), 6379–6390. https://doi.org/10.1021/acsami.6b00739.

Sefidkon, F., Jamzad, Z., 2005. Chemical composition of the essential oil of three Iranian Satureja species (S. mutica, S. macrantha and S. intermedia). Food Chem. 91 (1), 1–4. https://doi.org/10.1016/j.foodchem.2004.01.027.

Shi, R., Geng, H., Gong, M., Ye, J., Wu, C., Hu, X., Zhang, L., 2018. Long-acting and broad-spectrum antimicrobial electrospun poly (ε-caprolactone)/gelatin micro/nanofibers for wound dressing. J. Colloid Interface Sci. 509, 275–284. https://doi.org/10.1016/j.jcis.2017.08.092.

Shokrollahi, M., Bahrami, S.H., Nazarpak, M.H., Solouk, A., 2020. Multilayer nanofibrous patch comprising chamomile loaded carboxyethyl chitosan/poly(vinyl alcohol) and polycaprolactone as a potential wound dressing. Int. J. Biol. Macromol. 147, 547–559. https://doi.org/10.1016/j.ijbiomac.2020.01.067.

Si, W., Ni, X., Gong, J., Yu, H., Tsao, R., Han, Y., Chambers, J.R., 2009. Antimicrobial activity of essential oils and structurally related synthetic food additives towards Clostridium perfringens 106, 213–220. https://doi.org/10.1111/j.1365-2672.2008.03994.x.

Singh, S., Gupta, A., Sharma, D., Gupta, B., 2018. Dextran based herbal nanobiocomposite membranes for scar free wound healing. Int. J. Biol. Macromol. 113, 227–239. https://doi.org/10.1016/j.ijbiomac.2018.02.097.

Sofi, Hasham S., Akram, Towseef, Tamboli, Ashif H., Majeed, Aasiya, Shabir, Nadeem, Sheikh, Faheem A., 2019. Novel lavender oil and silver nanoparticles simultaneously loaded onto polyurethane nanofibers for wound-healing applications. Int. J. Pharm. 569, 118590. https://doi.org/10.1016/j.ijpharm.2019.118590.

Tampau, Alina, González-Martínez, Chelo, Chiralt, Amparo, 2020. Polyvinyl alcohol-based materials encapsulating carvacrol obtained by solvent casting and electrospinning. React. Funct. Polym. 153, 104603. https://doi.org/10.1016/j.reactfunctpolym.2020.104603.

Tawfik, Essam A., Craig, Duncan Q.M., Barker, Susan A., 2020. Dual drug-loaded coaxial nanofibers for the treatment of corneal abrasion. Int. J. Pharm. 581, 119296. https://doi.org/10.1016/j.ijpharm.2020.119296.

Tayel, Ahmed A., Moussa, Shaaban, El-Tras, Wael F., Knittel, Dierk, Opwis, Klaus, Schollmeyer, Eckhard, 2010. Anticandidal action of fungal chitosan against Candida albicans. Int. J. Biol. Macromol. 47 (4), 454–457. https://doi.org/10.1016/j.ijbiomac.2010.06.011.

Thangavel, P., Kannan, R., Ramachandran, B., Moorthy, G., Suguna, L., Muthuvijayan, V., 2018. Development of reduced graphene oxide (rGO)-isabgol nanocomposite dressings for enhanced vascularization and accelerated wound healing in normal and diabetic rats. J. Colloid Interface Sci. 517, 251–264. https://doi.org/10.1016/j.jcis.2018.01.110.

Victoria, Francine N., Radatz, Cátia S., Sachini, Maraísa, Jacob, Raquel G., Alves, Diego, Savegnago, Lucielli, Perin, Gelson, Motta, Amanda S., Silva, Wladimir P., Lenardão, Eder J., 2012. Further analysis of the antimicrobial activity of α-phenylseleno citronellal and α-phenylseleno citronellol. Food Control 23 (1), 95–99. https://doi.org/10.1016/j.foodcont.2011.06.017.

Vitanza, L., Maccelli, A., Marazzato, M., Scazzocchio, F., Comanducci, A., Fornarini, S., Crestoni, M.E., Filippi, A., Fraschetti, C., Rinaldi, F., Aleandri, M., Goldoni, P., Conte, M.P., Ammendolia, M.G., Longhi, C., 2019. Satureja montana L. essential oil and its antimicrobial activity alone or in combination with gentamicin. Microb. Pathog. 126, 323–331. https://doi.org/10.1016/j.micpath.2018.11.025.

Volpe, Caroline Maria Oliveira, Villar-Delfino, Pedro Henrique, dos Anjos, Paula Martins Ferreira, Nogueira-Machado, José Augusto, 2018. Cellular death, reactive oxygen species (ROS) and diabetic complications review-Article. Cell Death Dis. 9 (2) https://doi.org/10.1038/s41419-017-0135-z.

Wang, Lina, Liu, Fei, Jiang, Yanfeng, Chai, Zhi, Li, Pinglan, Cheng, Yongqiang, Jing, Hao, Leng, Xiaojing, 2011. Synergistic antimicrobial activities of natural essential oils with chitosan films. J. Agric. Food Chem. 59 (23), 12411–12419. https://doi.org/10.1021/jf203165k.

Yan, E., Fan, Y., Sun, Z., Gao, J., Hao, X., Pei, S., Wang, C., Sun, L., Zhang, D., 2014. Biocompatible core-shell electrospun nanofibers as potential application for chemotherapy against ovary cancer. Mater. Sci. Eng. C 41, 217–223. https://doi.org/10.1016/j.msec.2014.04.053.

Yang, Xinglong, Yang, Junchuan, Wang, Le, Ran, Bei, Jia, Yuexiao, Zhang, Lingmin, Yang, Guang, Shao, Huawu, Jiang, Xingyu, 2017. Pharmaceutical Intermediate-Modified Gold Nanoparticles: Against Multidrug-Resistant Bacteria and Wound-Healing Application via an Electrospun Scaffold. ACS Nano 11 (6), 5737–5745. https://doi.org/10.1021/acsnano.7b0124010.1021/acsnano.7b01240.s001.

Yousefi, I., Pakravan, M., Rahimi, H., Bahador, A., Farshadzadeh, Z., Haririan, I., 2017. An investigation of electrospun Henna leaves extract-loaded chitosan based nanofibrous mats for skin tissue engineering. Mater. Sci. Eng. C 75, 433–444. https://doi.org/10.1016/j.msec.2017.02.076.

Yuan, G., Chen, X., Li, D., 2016. Chitosan films and coatings containing essential oils: The antioxidant and antimicrobial activity, and application in food systems. Food Res. Int. 89, 117–128. https://doi.org/10.1016/j.foodres.2016.10.004.

Zhang, K., Bai, X., Yuan, Z., Cao, X., Jiao, X., Li, Y., Qin, Y., Wen, Y., Zhang, X., 2019a. Layered nanofiber sponge with an improved capacity for promoting blood coagulation and wound healing. Biomaterials 204, 70–79. https://doi.org/10.1016/j.biomaterials.2019.03.008.

Zhang, Yibo, Zhang, Ye, Zhu, Zhu, Jiao, Xiangyu, Shang, Yanli, Wen, Yongqiang, 2019b. Encapsulation of thymol in biodegradable nanofiber via coaxial eletrospinning and applications in fruit preservation. J. Agric. Food Chem. 67 (6), 1736–1741. https://doi.org/10.1021/acs.jafc.8b0636210.1021/acs.jafc.8b06362.s001.

Zomorodian, Kamiar, Moein, Mahmoodreza, Pakshir, Keyvan, Karami, Forough, Sabahi, Zahra, 2017. Chemical Composition and Antimicrobial Activities of the Essential Oil From Salvia mirzayanii Leaves. J. Evidence-Based Complement. Altern. Med. 22 (4), 770–776. https://doi.org/10.1177/2156587217717414.